American Mineralogist, Volume 72, pages 935–942, 1987

High-resolution ^{29}Si NMR spectroscopy of 2:1 layer silicates: Correlations among chemical shift, structural distortions, and chemical variations

CHARLES A. WEISS, JR., STEPHEN P. ALTANER, R. JAMES KIRKPATRICK
Mineral Physics Program, Department of Geology, University of Illinois, 245 Natural History Building, 1301 West Green Street, Urbana, Illinois 61801, U.S.A.

ABSTRACT

With increasing ^{IV}Al substitution and increasing total layer charge, the ^{29}Si NMR chemical shifts for specific types of $Q^3(n\text{Al})$ sites in 2:1 layer silicates become progressively deshielded (less negative). This deshielding is related to both structural distortions caused by mismatch of the tetrahedral and octahedral sheets and compositional variations in the octahedral sheet. One measure of structural distortion in 2:1 layer silicates, the amount of tetrahedral rotation within the crystallographic *a-b* plane, is linearly correlated with ^{29}Si chemical shift. As noted by previous authors, ^{29}Si chemical shifts in trioctahedral phyllosilicates are systematically more negative (more shielded) than ^{29}Si chemical shifts in analogous dioctahedral structures. This difference is apparently related to a greater total electronegativity of the octahedral cations coordinated to the apical oxygen in trioctahedral phases (three Mg^{2+} cations) as compared to dioctahedral phases (two Al^{3+} cations). One-for-one substitution of Mg for Al in dioctahedral phases and Li for Mg in trioctahedral phases (both of which increase negative 2:1-layer charge) causes deshielding at Si, apparently owing to a lower average electronegativity of the cations coordinated to the apical oxygen. Different interlayer cations cause only small changes in the ^{29}Si chemical shift. These correlations should be important in the structural analysis of smectite, vermiculite, illite, and mixed-layer clay minerals and provide information for these phases that is not easily obtainable from X-ray diffraction.

INTRODUCTION

This paper presents the results of a ^{29}Si MASS NMR (magic-angle sample-spinning nuclear magnetic resonance) spectroscopic study of phyllosilicate minerals (including clay minerals) that demonstrates that there are systematic relationships between the ^{29}Si NMR chemical shifts of specific $Q^3(n\text{Al})$ sites and compositional and structural parameters related to tetrahedral-sheet distortions for those phases. These parameters include ^{IV}Al substitution, total layer charge, and the amount of tetrahedral rotation within the crystallographic *a-b* plane. These relationships allow relatively easy, direct determination of these parameters, provide information about clay minerals that cannot be obtained by diffraction methods, and complement well the ability of ^{29}Si MASS NMR spectroscopy to provide data about the nature of short-range Al-Si order-disorder in phyllosilicates (Lipsicas et al., 1984; Herrero et al., 1985; Barron et al., 1985; Kirkpatrick and Weiss, 1987). Our results also confirm the systematic differences in ^{29}Si chemical shift between dioctahedral and trioctahedral phyllosilicates previously observed (Mägi et al., 1984; Sanz and Serratosa, 1984; Kirkpatrick et al., 1985).

The samples chosen for this study are monomineralic, Fe-poor, and chemically representative of most of the major subgroups of 2:1 layer silicates (Table 1). Both dioctahedral and trioctahedral phases were examined. Dioctahedral layer silicates have four octahedral cations and two vacancies per unit cell, and the cation is primarily Al^{3+}, whereas trioctahedral layer silicates have six octahedral cations per unit cell and the cation is primarily Mg^{2+} with or without Fe^{3+} and Fe^{2+}.

Throughout this paper we use the standard $Q^m(n\text{Al})$ notation for the local Si environment. In this notation, m = the number of bridging oxygens to which a Si is coordinated, and n = the number of tetrahedral Al (^{IV}Al) next-nearest neighbors to Si.

The ^{29}Si chemical-shift correlations for sheet silicates are broadly similar to those for framework silicates (e.g., Smith and Blackwell, 1983; Smith et al., 1984; Mägi et al., 1984; Kirkpatrick et al., 1985). For framework silicates, the best correlations relate the ^{29}Si chemical shift to average Si–O–T bond angle per tetrahedron (T = Si, Al), whereas for the sheet silicates (this study), the best correlations are with total layer charge and parameters related to the distortion of the tetrahedral sheet. Because we have the most data for $Q^3(0\text{Al})$ sites, we will only describe the correlations for these types of sites. There are also similar trends for the other $Q^3(n\text{Al})$ sites offset to less negative chemical shifts by 3 to 3.5 ppm due to ^{IV}Al for ^{IV}Si substitution (see, e.g., Kirkpatrick et al., 1985).

0003–004X/87/0910–0935$02.00

TABLE 1. Names, localities, structural formulae, fractions of ^{IV}Al substitution, and total layer charge for 2:1 silicates examined in this study

Name (ref.)*	Locality	Structural formula†	$^{IV}Al/(^{IV}Al + Si)$	Total layer charge
		Dioctahedral		
1. Pyrophyllite (1)	Robbins, North Carolina	$Al_4Si_8O_{20}(OH)_4$	0	0
2. Montmorillonite (2)	Crook County, Wyoming	$M^+_{0.70}[(Al_{2.99}Mg_{0.52}Fe^{3+}_{0.42}Fe^{2+}_{0.01})(Si_{7.97}Al_{0.03})O_{20}(OH)_4]$	0.004	0.70
3. Montmorillonite (3)	Apache County, Arizona (Cheto)	$M^+_{1.01}[(Al_{2.95}Mg_{0.76}Fe^{3+}_{0.25}Fe^{2+}_{0.04})(Si_{7.79}Al_{0.21})O_{20}(OH)_4]$	0.026	1.01
4. Montmorillonite (3)	Otay, California	$M^+_{1.25}[(Al_{2.69}Mg_{1.20}Fe^{3+}_{0.11})(Si_{7.95}Al_{0.05})O_{20}(OH)_4]$	0.0063	1.25
5. Montmorillonite (3)	Polkville, Massachusetts	$M^+_{1.28}[(Al_{2.78}Mg_{1.16}Fe_{0.20})(Si_{7.88}Al_{0.12})O_{20}(OH)_4]$	0.015	1.28
6. Montmorillonite (6)	Gonzales County, Texas	N.A.	N.A.	N.A.
7. Beidellite (4)	Black Jack mine, Idaho	$M^+_{1.10}[(Al_{3.91}Mg_{0.02}Fe_{0.06})(Si_{6.95}Al_{1.05})O_{20}(OH)_4]$	0.131	1.10
8. Muscovite (1)	Synthetic	$K_2[Al_4(Si_6Al_2)O_{20}(OH)_4]$	0.250	2.0
9. NH_4-mica (1)	Synthetic	$(NH_4)_2[Al_4(Si_6Al_2)O_{20}(OH)_4]$	0.250	2.0
10. Paragonite (1)	Synthetic	$Na_2[Al_4(Si_6Al_2)O_{20}(OH)_4]$	0.250	2.0
		Trioctahedral		
11. Talc (1)	N.A.	$Mg_6Si_8O_{20}(OH)_4$	0	0
12. Hectorite (4)	Hector, California	$M^+_{1.04}[(Mg_{4.70}Li_{1.15}Fe_{0.06})Si_8O_{20}(OH)_4]$	0	1.04
13. Saponite (4)	Ballarat, California	$M^+_{0.98}[(Mg_{5.79}Al_{0.12}Fe_{0.07})(Si_{6.85}Al_{1.15})O_{20}(OH)_4]$	0.144	0.98
14. Fluorophlogopite (1)	Synthetic	$K_2[Mg_6(Si_6Al_2)O_{20}(OH,F)_4]$	0.250	2.0
15. Mg-vermiculite (5)	Llano County, Texas	$M^+_{1.97}[(Mg_{5.66}Al_{0.30}Fe_{0.02})(Si_{5.72}Al_{2.28})O_{20}(OH)_4]$	0.285	1.97
16. Chlorite (6)	New S. Wales, Australia	N.A.	0.224	N.A.

Note: N.A. = not available.

* Reference for chemical analysis: (1) Assumed stoichiometric composition; (2) Stucki et al. (1984); (3) Schultz (1969); (4) Callaway and McAtee (1985); (5) Shirozu and Bailey (1966); (6) Chemical analysis not available.

† Sources of chemical analyses are from references noted in column one.

EXPERIMENTAL DETAILS

The ^{29}Si NMR spectra were obtained at a frequency of 71.5 MHz with a "home-built" Fourier-transform NMR spectrometer based on a 8.45-T, 3.5-in.-bore solenoid (Oxford Instruments, Osney Mead, Oxford, England) and a variety of digital and radiofrequency electronics, including a Nicolet (Madison, Wisconsin) 1280 data system, 293B pulse programmer, and a Diablo model 40 disc system for data storage (Diablo Systems, Inc., Haywood, California). The experimental conditions were similar to those of K. A. Smith et al. (1983), except that tetramethylsilane (TMS) was used as an external chemical-shift standard. The ^{29}Si chemical shifts are reported in parts per million (ppm) relative to TMS. Our chemical shifts are similar to those previously published, but to minimize uncertainty due to interlaboratory standardization (about 1 ppm), we use only our data and those of Lipsicas et al. (1984) for saponites in the correlations.

X-ray diffraction data were determined using a Siemens D-500 powder diffractometer with Cu$K\alpha$ radiation. The b-axis dimensions were measured using the d_{060} peak. Goniometer speed was 0.50° 2θ/min.

TABLE 2. Approximate lateral dimensions (b_{ideal}) of unconstrained octahedral and tetrahedral sheets

Composition	Mineral	b_{ideal} (Å)	Example
$Al(OH)_3$	Gibbsite, bayerite	8.64, 8.67	
$Mg(OH)_2$	Brucite	9.36	
Si_4O_{10}		9.15*	Pyrophyllite, talc, hectorite, montmorillonite
$(Si_3Al)O_{10}$		9.335*	Muscovite, phlogopite
$(Si_2Al_2)O_{10}$		9.52*	Margarite
$(SiAl_3)O_{10}$		9.705*	Clintonite

Note: Adapted from Guggenheim (1984).

* b_{ideal} from $b(Si_{1-x}Al_x) \simeq 9.15$ Å $+ 0.74x$.

A number of smectite and vermiculite samples were Cs saturated by reacting 0.5–1.0 g of clay with about 50 mL 0.1M CsBr solution at 60°C for 2 h; the process was repeated for a total of three times with fresh solutions. The samples were then rinsed in distilled water three times. After rinsing, the samples were dried in an oven at 60°C.

STRUCTURAL DISTORTIONS IN 2:1 LAYER SILICATES

Because much of the variation in ^{29}Si NMR chemical shifts in layer silicates appears to correlate with distortions in the tetrahedral sheet, we present a brief description of these distortions in 2:1 layer silicates. Distortions occur because most layer silicates have tetrahedral sheets with ideal lateral dimensions (a and b axis) that are different from the ideal lateral dimensions of their octahedral sheet and because layer silicates have planes of oxygen atoms shared by both sheets. To fit the sheets together, the lateral dimensions of both sheets must be the same, and thus, the sheets become distorted.

Table 2 gives b-axis dimensions for unconstrained octahedral and tetrahedral sheets from Guggenheim (1984). Free octahedral sheets exist in hydroxide minerals such as gibbsite and brucite, and these are used to estimate the b-axis dimensions of ideal octahedral sheets in layer silicates. Although free tetrahedral sheets do not exist, ideal b-axis dimensions (shown in Table 2) can be calculated using Al–O bond lengths of 1.748 and Si–O bond lengths of 1.618 with hexagonal geometry (Bailey, 1980). The b-axis dimensions of ideal tetahedral sheets increase systematically with increasing ^{IV}Al substitution. Structural analyses indicate that tetahedral sheets are larger than octahedral sheets in all 2:1 layer silicates, including talc (Bailey, 1980), suggesting that either actual Si–O bond

TABLE 3. Structural parameters for 2:1 layer silicates examined in this study

Name (ref.)*	b_{obs} (Å)	b_{ideal} (Å)	α_{calc} (°)	α_{meas} (°)	τ (°)	avg. T–O (Å)	b'_{ideal} (Å)
			Dioctahedral				
1. Pyrophyllite (1)	8.955	9.150	11.9	10.2	109.4	1.62	9.16
2. Wyoming montmorillonite	8.986	9.153	11.0				
3. Cheto montmorillonite	8.993	9.169	11.2				
4. Otay montmorillonite	8.999	9.155	10.6				
5. Polkville montmorillonite	8.993	9.161	11.0				
6. Texas montmorillonite	8.999	9.155	10.6				
7. Beidellite	8.954	9.247	14.5				
8. Muscovite (2)	8.995	9.335	15.5	11.4	111.1	1.64	9.28
9. NH_4-mica	9.024	9.335	14.8				
10. Paragonite (3)	8.896	9.335	17.6	16.2	110.4	1.65	9.33
			Trioctahedral				
11. Talc (4)	9.166	9.150	0	3.4	109.2	1.62	9.16
12. Hectorite	9.099	9.150	6.1				
13. Saponite	9.188	9.250	6.6				
14. Fluorophlogopite (5)	9.201	9.335	9.7	7.5	110.5	1.64	9.28
15. Mg-vermiculite (6)	9.222	9.361	9.9	5.7	110.5	1.65	9.33
16. Chlorite (7)	9.201	9.316	9.0	6.4	110.7	1.65	9.33

Note: Parameters include b_{obs}, b_{ideal}, α_{calc}, α_{meas}, τ, average T–O bond lengths, and b'_{ideal}. Sources of structure refinements from noted references.

* (1) Lee and Guggenheim (1981); (2) Güven (1971); (3) Lin and Bailey (1984); (4) Rayner and Brown (1973); (5) Hazen and Burnham (1973);(6) Shirozu and Bailey (1966); (7) Joswig et al. (1980).

lengths in certain phyllosilicates are larger than the values assumed in Table 2 or that the octahedral sheet in Mg-trioctahedral phases is smaller than that of brucite.

In phyllosilicates, there are three ways in which the lateral dimensions of the tetrahedral sheet may be reduced to match the size of the octahedral sheet: (1) rotation of adjacent tetrahedra in opposite directions within the *a*-*b* plane (Zvyagin, 1957; Radoslovich, 1961), (2) thickening of the tetrahedral sheet in the *c**-axis direction by increasing the O_{apical}–tetrahedral cation–O_{basal} bond angle (Bailey, 1980), and (3) decreasing Si–O bond lengths.

The amount of tetrahedral rotation is described by the average deviation (α) of the T–O–T (tetrahedral cation–basal oxygen–tetrahedral cation) angle from hexagonal symmetry. An α value of 0° represents undistorted tetrahedral sheets, and α may increase to a theoretical maximum value of 30°. The value of α_{meas} is directly measured from a structural refinement, and α_{calc} is determined using the relationship $\cos \alpha_{calc} = b_{obs}/b_{ideal}$, where b_{obs} is the *b*-axis dimension measured using XRD data and b_{ideal} is determined using the relationship given in Table 2.

For example, given a stoichiometric muscovite composition, $b_{ideal} = b_{Si_{0.75}Al_{0.25}} = 9.335$, and from Table 3, $b_{obs} = 8.995$. Therefore, $\alpha_{calc} = \cos^{-1}(8.995/9.335) = 15.5°$. Table 3 lists b_{obs}, b_{ideal}, α_{calc}, and α_{meas} values for the minerals examined in this study. Because stacking disorder and fine grain size limit structural refinements of clay minerals, there are structural refinements, and therefore α_{meas} values, for only seven minerals examined in this study.

The lateral dimensions of a tetrahedral sheet can be reduced by an increase in the average apical oxygen–tetrahedral cation–basal oxygen bond angle (τ), the amount of reduction being measured by the difference between τ for an ideal tetrahedron and the observed value. An undistorted tetrahedron has a τ value of 109°28′. The seven τ values listed in Table 3 are determined from structural refinements. Because τ must be obtained from structural refinements, it is not available for most clay minerals.

Finally, the lateral dimensions of a tetahedral sheet may be reduced by decreasing T–O bond lengths. Hexagonal geometry and Si–O and Al–O bond lengths of 1.618 and 1.748 Å, respectively, were assumed in the calculation of b_{ideal}. Measured T–O bond lengths (Table 3) represent average values including both Si–O and Al–O and allow an alternative method of calculating undistorted *b*-axis di-

TABLE 4. ^{29}Si MASS NMR chemical shifts for $Q^3(n\text{Al})$ sites in 2:1 layer silicates examined in this study

Name	Q^3(0Al)	Q^3(1Al)	Q^3(2Al)	Q^3(3Al)
	Dioctahedral			
1. Pyrophyllite	−95.9			
2. Wyoming montmorillonite	−93.5			
Cs^+-saturated	−93.7			
3. Cheto montmorillonite	−94.1			
Cs^+-saturated	−94.1			
4. Otay montmorillonite	−93.4			
Cs^+-saturated	−93.6			
5. Polkville montmorillonite	−93.3			
6. Texas montmorillonite	−93.6			
Cs^+-saturated	−94.1			
7. Beidellite	−92.6	−88.4		
Cs^+-saturated	−93.0	−88.5		
8. Muscovite	−89.5	−86.5	−83.0	
9. NH_4-mica	−90.5	−87.1	−84.1	
10. Paragonite	−88.9	−84.2	−80.6	
	Trioctahedral			
11. Talc	−98.5			
12. Hectorite	−94.2			
Cs^+-saturated	−94.9			
13. Saponite	−95.6	−90.7	−84.8	
Cs^+-saturated	−95.6	−91.0	−85.0	
14. Fluorophlogopite	−92.9	−89.2	−85.6	
15. Mg-vermiculite	−92.9	−88.7	−84.6	
Cs^+-saturated	−92.8	−89.2	−85.3	
16. Chlorite	−91.2	−87.0	−83.2	−79.4

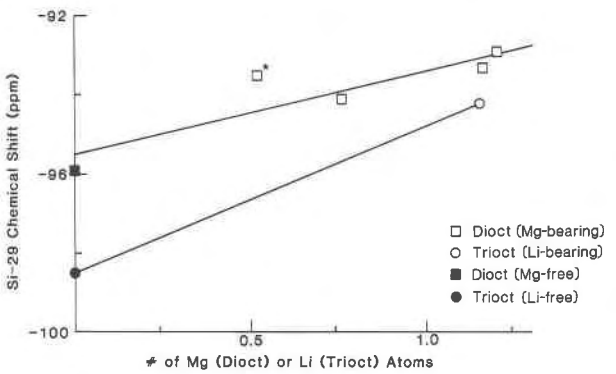

Fig. 1. ^{29}Si chemical shifts of $Q^3(0Al)$ sites vs. either number of $^{VI}Mg^{2+}$ cations in dioctahedral clays (open square symbols) or $^{VI}Li^{+}$ cations in trioctahedral clays (open circle symbols). Samples with nearly pure Si tetrahedral sheets and octahedral sheets of variable composition are plotted with closed symbols (pyrophyllite and talc). Lines in this figure and all others are least-squares fits to the available data points (Table 5). The point marked with a * is Wyoming montmorillonite, for which the higher Fe content may cause a less negative chemical shift due to paramagnetic effects.

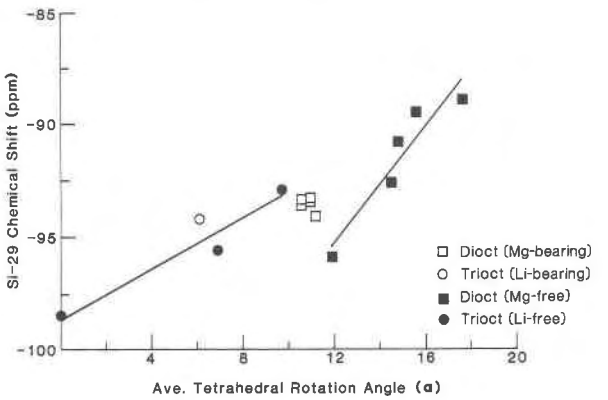

Fig. 2. ^{29}Si chemical shifts of $Q^3(0A1)$ sites vs. calculated average tetrahedral rotation angle (α) in trioctahedral and dioctahedral phyllosilicates. Open symbols represent samples with significant octahedral substitution, and solid symbols represent samples with no substitution of Li for Mg (trioct.), or Mg for Al (dioct.).

mensions using the equation $b'_{ideal} = 4(2)^{1/2}$(T–O) (Bailey, 1980). The b'_{ideal} values are similar to b_{ideal} values (Table 3), and it seems likely that the individual Si–O and Al–O bond lengths in clay-mineral structures are similar to the assumed values of 1.618 and 1.748 Å, respectively.

Results and Discussion

Effects of octahedral cations

The ^{29}Si NMR chemical shifts of our samples (Table 4) support the observations of Mägi et al. (1984) and Kirkpatrick et al. (1985) that Mg-trioctahedral phases have more shielded (more negative) chemical shifts than their dioctahedral counterparts. For minerals that differ only by the composition of the octahedral sheet, the chemical shift of the Mg-trioctahedral phase is always 2–3 ppm more negative (described by the chemical-shift difference, Δ; e.g., for muscovite and fluorophlogopite, $\Delta = 3.4$; for pyrophyllite and talc, $\Delta = 2.6$; for beidellite and saponite, $\Delta = 2.7$). This relationship holds for Si in each type of $Q^3(n\text{Al})$ site.

These differences can be related to the electronegativity of the other cations to which the oxygen atoms of a Si tetrahedron are coordinated, which in turn affects the degree of *s* hybridization of the oxygen-bond orbitals (Engelhardt and Radeglia, 1984). Based on simple quantum-chemical calculations that take into account the paramagnetic contribution to the chemical shift (Engelhardt and Radeglia, 1984, and references therein), the chemical shift becomes more shielded as the cation electronegativity (EN) increases. This relationship is $\delta = -a\text{EN} + b$, where δ is the ^{29}Si chemical shift and a and b are empirical constants.

The Si sites in Mg-rich trioctahedral phases differ from those in Al-dioctahedral phases in that each apical oxygen is coordinated to 3 Mg atoms rather than 2 Al atoms. The total electronegativity of the cations in the octahedral sheet coordinated to the apical oxygens is 3.6 (3Mg × 1.2) for pure trioctahedral phases compared to 3 (2Al × 1.5) for pure dioctahedral phases. For phases with similar tetrahedral sheets, then, the shielding at Si should be greater for trioctahedral phases than for dioctahedral phases, in agreement with the observed relationships.

Similarly, for minerals with a fixed octahedral occupancy (i.e., two in dioctahedral phases or three in trioctahedral phases), *atom-for-atom* substitution of an element with a lower electronegativity should cause a corresponding deshielding at Si. Because Mg (EN = 1.2) is less electronegative than Al (EN = 1.5), substitution of 1 Mg atom for 1 Al atom in the octahedral sheet of a dioctahedral mineral should cause deshielding at Si. One-for-one substitution of Li (EN = 1.0) for Mg in a trioctahedral mineral should have the same effect. These predictions are consistent with observed variations (Fig. 1). For trioctahedral phases, one-for-one Li-for-Mg substitution (i.e., in hectorite vs. talc) causes about a 4 ppm deshielding, and for dioctahedral phases (the montmorillonites vs. pyrophyllite), one-for-one Mg-for-Al substitution causes about a 2 ppm deshielding. Because the octahedral occupancy remains constant, this atom-for-atom substitution increases negative 2:1-layer charge.

The only sample that does not fit the general trend for the dioctahedral minerals in Figure 1 (Wyoming montmorillonite) has a significantly deshielded ^{29}Si chemical shift relative to the other montmorillonites. We interpret this deshielding to be due to the relatively large substitution of Fe^{3+} into the octahedral sheet of this sample causing a paramagnetic deshielding at Si. Such a paramagnetic deshielding due to Fe-for-Mg substitution also occurs in olivines (Grimmer et al., 1983).

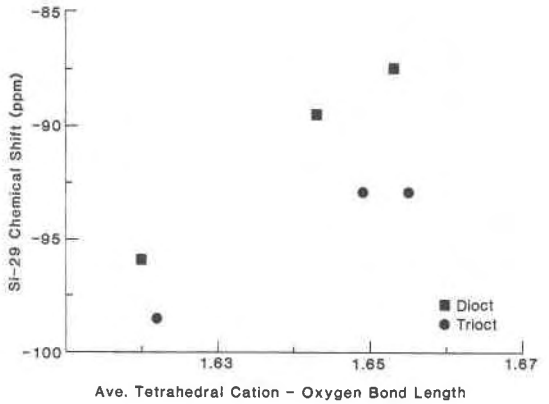

Fig. 3. ^{29}Si chemical shifts of $Q^3(0Al)$ sites vs. average tetrahedral cation–oxygen bond length in trioctahedral and dioctahedral sheet silicates.

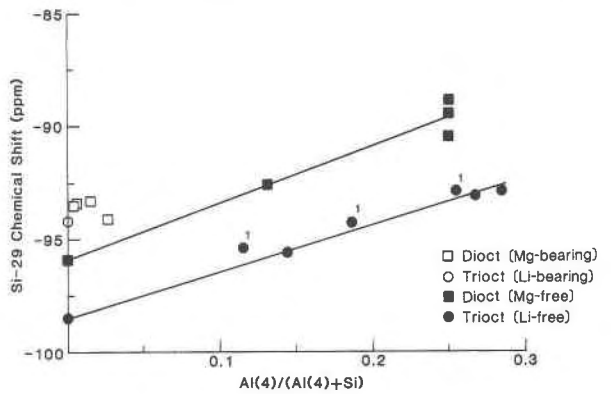

Fig. 4. ^{29}Si chemical shifts of $Q^3(0Al)$ sites vs. amount of ^{IV}Al substitution in trioctahedral and dioctahedral sheet silicates. Symbols labeled with "1" are saponites from Lipsicas et al. (1984).

Correlations with tetrahedral distortions

As for framework silicates (e.g., K. A. Smith et al., 1983, J. V. Smith et al., 1984; Mägi et al., 1984), the ^{29}Si chemical shifts for phyllosilicates vary systematically with several structural parameters. Because trioctahedral phases are more shielded than dioctahedral phases (as discussed above), there are separate correlations for dioctahedral and trioctahedral phases.

The ^{29}Si chemical shifts for $Q^3(0Al)$ sites generally show progressive deshielding with increasing distortion of the tetrahedral sheet as measured by α_{calc} (Fig. 2). For trioctahedral phases, this correlation is well defined. For dioctahedral phases, the relationship is also well defined except for the montmorillonite samples, which show the reverse trend. The ^{29}Si chemical shifts also show progressive deshielding with increasing α_{meas} values (Tables 3 and 4), although the data are limited.

For all the phases except the montmorillonites, increased α values are caused by substitution of Al^{3+} for Si^{4+} in the tetrahedral sheet and, to a lesser extent, by changes in the interlayer cation.

The differing trend for the montmorillonite samples appears to be related to differences in the composition of the octahedral sheet in these minerals. Pyrophyllite and the Wyoming, Cheto, Polkville, and Otay montmorillonites represent a series of dioctahedral phases with nearly pure Si-tetrahedral sheets, but with increasing Mg^{2+}-for-Al^{3+} substitution in the octahedral sheet (Table 1). As described above, this atom-for-atom substitution retains the dioctahedral character of the mineral and develops a larger negative 2:1-layer charge. Because these samples contain no detectable ^{IV}Al, their ideal tetrahedral sheets should have the same size. However, the substitution of Mg^{2+} for Al^{3+} in the octahedral sheet causes an enlargement of the octahedral sheet due to the larger ionic radius of Mg^{2+} (0.80 Å) relative to Al^{3+} (0.61 Å). This expansion of the octahedral sheet reduces the mismatch between the tetrahedral and octahedral sheets, thereby reducing the α value. Simultaneously, the increasing Mg content of the octahedral sheet causes a deshielding at Si due to the decreasing average electronegativity of the octahedral cations coordinated to the apical oxygen.

We expected to find that the ^{29}Si chemical shifts of both dioctahedral and trioctahedral phases become progressively deshielded with increasing τ, and there does appear to be a rough trend (Tables 3 and 4). Talc for instance, has the least distorted tetrahedron (lowest τ) and the most shielded (negative) chemical shift. Paragonite and muscovite have larger τ values and less shielded chemical shifts. Because we have not examined the same samples for which the structure refinements were obtained and because there is a large range of τ values for the same phase (Bailey, 1984), this correlation is at present poorly defined.

The ^{29}Si chemical shift also seems to become deshielded with increasing average T–O bond length (Fig. 3), but there are few reliable data. As discussed above, individual Si–O and Al–O bond lengths appear to be relatively constant for these six minerals in Figure 3. Hence, the deshielding with increasing average T–O bond length in Figure 3 may simply reflect deshielding due to increasing tetrahedral distortion caused by greater ^{IV}Al substitution.

Correlations with ^{IV}Al/(Si + ^{IV}Al) and total layer charge

For minerals with the same type of octahedral sheet, ^{IV}Al-for-Si substitution is the main cause of distortion in the tetrahedral sheet and, thus, correlates well with progressively deshielded ^{29}Si chemical shifts (Fig. 4). The data for the Mg-rich trioctahedral phases (talc, saponite, fluorophlogopite, and vermiculite) fall along the lower line in Figure 4, which also includes the data of Lipsicas et al. (1984) for synthetic saponites. The data for the dioctahedral phases (pyrophyllite, beidellite, muscovite, NH_4-mica, and paragonite) fall along the upper line. The data for dioctahedral and trioctahedral smectites with nearly no ^{IV}Al substitution, but with significant Mg^{2+}-for-Al^{3+} or Li^{+}-for-Mg^{2+} substitution, cluster between −95 and −93 ppm (open symbols in Fig. 4). As discussed above, the

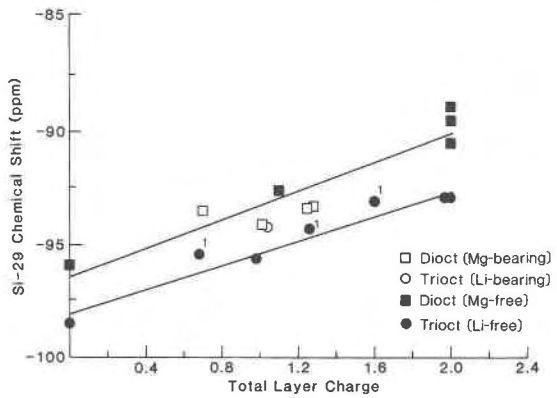

Fig. 5. ^{29}Si chemical shifts of Q^3(0Al) vs. total layer charge in trioctahedral and dioctahedral sheet silicates. Symbols marked with "1" are saponites from Lipsicas et al. (1984).

^{29}Si chemical shifts of these minerals are deshielded because of compositional variations in the octahedral sheet (Fig. 1). These separate trends for dioctahedral and trioctahedral phases parallel the separate trends of deshielding at ^{27}Al with decreasing Si/(Si + ^{IV}Al) in dioctahedral and trioctahedral sheet silicates (Kinsey et al., 1985).

The ^{29}Si chemical shifts also become systematically deshielding with increasing total layer charge (Fig. 5). For trioctahedral phases, total layer charge increases owing to tetrahedral Al-for-Si substitution and octahedral Li-for-Mg substitution, whereas for dioctahedral phases, total layer charge increases owing to tetrahedral Al-for-Si substitution and octahedral Mg-for-Al substitution. As discussed above, all of these substitutions cause deshielding at Si. Because substitutions in both the octahedral and tetrahedral sheets produce an approximately similar amount of deshielding at Si, the chemical shifts for the montmorillonite and hectorite samples, which correlate poorly with ^{IV}Al/(Si + ^{IV}Al) (Fig. 4), correlate much better with total layer charge.

Effects of the interlayer cation

The dioctahedral micas with similar tetrahedral Al substitution and overall layer charge (muscovite, NH_4-mica, and paragonite) have slightly different ^{29}Si chemical shifts (up to 1.6 ppm) for their Q^3(0Al) sites. These differences appear to be related to differences in α caused by differences in the radii of the interlayer cations. Because Na^+ (1.02 Å in 6-fold coordination, Shannon and Prewitt, 1969) is smaller than K^+ (1.37 Å in 6-fold coordination, Shannon and Prewitt, 1969) or NH_4^+ (1.61 Å in 6-fold coordination, Khan and Baur, 1972), the oxygen framework rotates slightly to coordinate more closely with Na^+, causing a larger α value for paragonite and a slightly less shielded ^{29}Si chemical shift relative to muscovite or NH_4-mica. These distortions allow the interlayer cation to be 6-fold coordinated by oxygen.

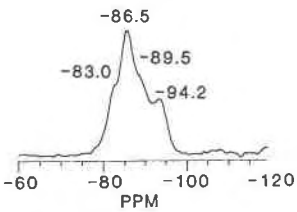

Fig. 6. ^{29}Si MASS NMR spectrum of a synthetic illite with 3% smectite layers. The peak at −94.2 ppm is smectite Q^3(0Al), the peak at −86.5 ppm is illite Q^3(1Al), and peak at −83.0 ppm is illite Q^3(2Al). Smectite Q^3(1Al) and illite Q^3(0Al) peaks overlap at about −89.5 ppm.

The effect of varying exchangeable cations in the interlayers of clays appears to be small, although we have examined the effect of only Cs^+. The ^{29}Si chemical shifts of the Cs^+-saturated samples (Table 4) show small and nonsystematic differences from those of the natural samples, which probably contain mostly Na^+ or Ca^{2+} in the interlayer. Thompson (1984) found similar results for a montmorillonite sample exchanged with a variety of cations. Cs^+ (1.70 Å in 6-fold coordination, Shannon and Prewitt, 1969) is larger than the common interlayer cations of clay minerals (Na, Ca, or K). If the effects of the interlayer cation were significant, they should be greatest for the Cs^+-saturated samples owing to heavy-atom effects, as discussed by Webb (1983). In the heavy-atom effect, the nuclear shielding of a lighter atom (e.g., Si) is influenced by a change in its electronic energy levels due to spin-orbit coupling interactions from a neighboring heavy nucleus (e.g., Cs). The magnitude of the interaction depends approximately on the fourth power of the nuclear charge.

TABLE 5. Coefficients and constants for linear-regression correlations of ^{29}Si chemical shifts (δ^{29}Si) vs. structural and compositional parameters (P)

Relationship	a	b	R^2
^{VI}Mg substitution (dioct.)	2.132	−95.492	0.806
Tetrahedral rotation (dioct.)	1.297	−110.843	0.897
Tetrahedral rotation (trioct.)	0.572	−98.734	0.959
^{IV}Al substitution (dioct.)	25.052	−95.894	0.960
^{IV}Al substitution (trioct.)	20.601	−98.498	0.991
Total layer charge (dioct.)	3.198	−96.441	0.875
Total layer charge (trioct.)	2.731	−98.092	0.935

Note: Equations are of the form $\delta^{29}Si = aP + b$ (see Figs. 1, 2, 4, and 5 for plots).

Applications and conclusions

The results of this work and previous studies show clearly that variations in the ^{29}Si chemical shifts of phyllosilicate phases are closely related to the amount of structural distortion of the tetrahedral sheet, and to the chemical variations in the octahedral and tetrahedral sheets, and that the effects of exchangeable interlayer cations are small. Previous investigations have demonstrated the well-known deshielding at Si with increasing number of ^{IV}Al next-nearest neighbors (e.g, Kirkpatrick et al., 1985).

Because of these relationships, the compositional parameters Si/(Si + ^{IV}Al) and total layer charge can be es-

timated quite well from the ^{29}Si $Q^3(n\text{Al})$ chemical shifts (Table 5). Layer charge in smectites and vermiculites is closely related to properties such as swelling, cation-exchange capacity, and catalysis. NMR analysis provides an important new method of determination of layer charge in these minerals.

In addition, NMR analysis of layer charge has important applications to petrologic studies of clay minerals such as mixed-layer illite/smectite. Development of high layer charge in the smectite component of illite/smectite has been suggested to occur in K-deficient environments, including deeply buried sandstones (Howard, 1981) and altered basalts (Howard and Roy, 1985). Using ^{29}Si NMR data, layer charge of the illite and smectite components of illite/smectite can be estimated independently.

An example of this latter application is the interpretation of the ^{29}Si NMR spectrum of a synthetic illite with 3% smectite layers as determined by X-ray diffraction (Fig. 6). The smectite Q^3(0Al) peak has a chemical shift of -94.2 ppm, and the illite Q^3(1Al) peak has a chemical shift of -86.4 ppm, similar to that for muscovite (Komarneni et al., 1986). In this analysis, we use the Q^3(1Al) peak of illite because the smectite Q^3(1Al) and illite Q^3(0Al) peaks overlap. The chemical shifts indicate a total layer charge per formula unit of 0.75 for the smectite component and 2.0 for the illite component, in agreement with the Al-rich composition of the starting gel. The inversion recovery technique of Barron et al. (1985) allows separate detection of the illite and smectite peaks and may make similar interpretations even more useful.

The results reported here also verify the differences in ^{29}Si chemical shifts between trioctahedral and dioctahedral 2:1 phyllosilicates of similar total layer charge and tetrahedral-sheet composition. We interpret this increased shielding for trioctahedral phases to be due to the effect of increased electronegativity of the cations coordinated to the apical oxygen of the Si tetrahedron. In addition, we have found that atom-for-atom substitution of ^{VI}Mg for ^{VI}Al in dioctahedral phases and ^{VI}Li for ^{VI}Mg in trioctahedral phases produces significant deshielding at Si consistent with a decrease in the average electronegativity of the cations coordinated to the apical oxygen. Quantitative corroboration of these ideas based on quantum-chemical calculations is needed but difficult at present (Tossell and Lazzeretti, 1986). The relatively large differences in ^{29}Si chemical shift between di- and trioctahedral phases may help to understand better whether smectite minerals from saline and alkaline lakes consist of separate dioctahedral and trioctahedral phases or one phase of intermediate character (e.g., Jones and Weir, 1983).

Acknowledgments

We thank Eric Daniels for running XRD patterns of the samples and Norma Vergo for supplying some of the samples. This work was supported by NSF Grant EAR-8408421 and a grant from Texaco.

Reviews by Bernard deJong and an anonymous reviewer significantly improved an earlier version of this paper.

References

Bailey, S.W. (1980) Structures of layer silicates. In G.W. Brindley and G. Brown, Eds., Crystal structures of clay minerals and their X-ray identification, p. 1–124. Mineralogical Society, London.

——— (1984) Crystal chemistry of the true micas. Mineralogical Society of America Reviews in Mineralogy, 13, 13–60.

Barron, P.F., Slade, P., and Frost, R.L. (1985) Ordering of aluminum in tetrahedral sites in mixed-layer 2:1 phyllosilicates by solid-state high-resolution NMR. Journal of Physical Chemistry, 89, 3880–3885.

Callaway, W.S., III, and McAtee, J.L., Jr. (1985) Magnetic susceptibilities of representative smectites. American Mineralogist, 70, 996–1003.

Engelhardt, G., and Radeglia, R. (1984) A semi-empirical quantum-chemical rationalization of the correlation between SiOSi angles and ^{29}Si NMR chemical shifts of silica polymorphs and framework aluminosilicates (zeolites). Chemical Physics Letters, 108, 271–274.

Grimmer, A.D., von Lampe, F., Mägi, M., and Lippmaa, E. (1983) Hochauflösende ^{29}Si NMR an festen silicaten; Einfluss von Fe^{2+} in olivinen. Zeitschrift für Chemie, 23, 343–344.

Guggenheim, S. (1984) The brittle micas. Mineralogical Society of America Reviews in Minerology, 13, 61–104.

Güven, N. (1971) The crystal structures of $2M_1$ phengite and $2M_1$ muscovite. Zeitschrift für Kristallographie, 134, 196–212.

Hazen, R.M., and Burnham, C.W. (1973) The crystal structures of one-layer phlogopite and annite. American Mineralogist, 58, 889–900.

Herrero, C.P., Sanz, J., and Serratosa, J.M. (1985) Tetrahedral cation ordering in layer silicates by ^{29}Si NMR spectroscopy. Solid State Communication, 53, 151–154.

Howard, J.J. (1981) Lithium and potassium saturation of illite/smectite clays from interlaminated shales and sandstones. Clays and Clay Minerals, 29, 136–142.

Howard, J.J., and Roy, D.M. (1985) Development of layer charge and kinetics of experimental smectite alteration. Clays and Clay Minerals, 33, 81–88.

Jones, B.F., and Weir, A.H. (1983) Clay minerals of Lake Abert, an alkaline, saline lake. Clays and Clay Minerals, 31, 161–172.

Joswig, W., Fuess, H., Rothbauer, R., Takéuchi, Y., and Mason, S.A. (1980) A neutron diffraction study of a one-layer triclinic chlorite (penninite). American Mineralogist, 65, 349–352.

Khan, A.A., and Baur, W. H. (1972) Salt hydrates, VIII. The crystal structures of sodium ammonium orthochromate dihydrate and magnesium diammonium bis (hydrogen orthophosphate) tetrahydrate and a discussion of the ammonium ion. Acta Crystallographica, B28, 683–693.

Kinsey, R.A., Kirkpatrick, R.J., Hower, J., Smith, K.A., and Oldfield, E. (1985) High-resolution aluminum-27 and silicon-29 nuclear magnetic resonance spectroscopic study of layer silicates, including clay minerals. American Mineralogist, 70, 537–548.

Kirkpatrick, R.J., and Weiss, C.A., Jr. (1987) Magic-angle sample-spinning NMR spectroscopy of clay minerals. In J.V. Stucki, Ed., Advanced chemical methods in soil and clay minerals research. D. Reidel Publishers, Boston, Massachusetts, in press.

Kirkpatrick, R.J., Smith, K.A., Schramm, S., Turner, G., and Yang, W.-H. (1985) Solid-state nuclear magnetic resonance spectroscopy of minerals. Annual Review of Earth and Planetary Science, 13, 29–47.

Komarneni, S., Fyfe, C.A., Kennedy, G.J., and Strobl, H. (1986) Characterization of synthetic and naturally occurring clays by ^{27}Al and ^{29}Si magic-angle spinning NMR spectroscopy. Journal of the American Chemical Society, 69, C-45–C-47.

Lee, J.H., and Guggenheim, S. (1981) Single crystal x-ray refinement of pyrophyllite-$1T_c$. American Mineralogist, 66, 350–357.

Lin, C.-yi, and Bailey, S.W. (1984) The crystal structure of paragonite-$2M_1$. American Mineralogist, 69, 122–127.

Lipsicas, M., Raythatha, R.H., Pinnavaia, T.J., Johnson, I.D., Giese, R.F., Costanzo, P.M., and Robert, J.-L. (1984) Silicon and aluminum site distributions in 2:1 layered silicate clays. Nature, 309, 604–609.

Mägi, M., Lippmaa, E., Samoson, A., Engelhardt, G., and Grimmer, A.-R. (1984) Solid-state high-resolution silicon-29 chemical shifts in silicates. Journal of Physical Chemistry, 88, 1518–1522.

Radoslovich, E.W. (1961) Surface symmetry and cell dimensions of layer lattice silicates. Nature, 191, 67–68.

Rayner, J.H., and Brown, G. (1973) The crystal structure of talc. Clays and Clay Minerals, 21, 103–114.

Sanz, J., and Serratosa, J.M. (1984) ^{29}Si and ^{27}Al high-resolution MAS-NMR spectra of phyllosilicates. American Chemical Society Journal, 106, 4790–4793.

Schultz, L.G. (1969) Lithium and potassium absorption, dehydroxylation temperature, and structural water content of aluminous smectites. Clays and Clay Minerals, 17, 115–149.

Shannon, R.D., and Prewitt, C.T. (1969) Effective ionic radii in oxides and fluorides. Acta Crystallographica, B25, 925–946.

Shirozu, H., and Bailey, S.W. (1966) Crystal structure of a 2-layer Mg-vermiculite. American Mineralogist, 51, 1124–1143.

Smith, J.V., and Blackwell, C.S. (1983) Nuclear magnetic resonance of silica polymorphs. Nature, 303, 223–225.

Smith, J.V., Blackwell, C.S., and Hovis, C.L. (1984) NMR of albite-microcline series. Nature, 309, 140–142.

Smith, K.A., Kirkpatrick, R.J., Oldfield, E., and Henderson, D.M. (1983) High-resolution silicon-29 nuclear magnetic resonance spectroscopic study of rock-forming silicates. American Mineralogist, 68, 1206–1215.

Stucki, J.W., Golden, D.C., and Roth, C.B. (1984) Effects of reduction and reoxidation of structural iron on the surface charge dissolution of dioctahedral smectites. Clay and Clay Minerals, 32, 350–356.

Thompson, J.G. (1984) ^{29}Si and ^{27}Al nuclear magnetic resonance spectroscopy of 2:1 clay minerals. Clay Minerals, 19, 229–236.

Tossell, J.A., and Lazzeretti, P. (1986) Ab initio calculations of ^{29}Si chemical shifts of some gas phase and solid state silicon fluorides and oxides. Journal of Chemical Physics, 84, 369–374.

Webb, G.A. (1983) Factors contributing to the observed chemical shifts of heavy nuclei. In NMR of newly accessible nuclei, vol. 1, p. 79–89. Academic Press, New York.

Zvyagin, B.B. (1957) Determination of the structure of celadonite by electron diffraction. Soviet Physics Crystallography, 2, 388–394.

MANUSCRIPT RECEIVED SEPTEMBER 10, 1986
MANUSCRIPT ACCEPTED MAY 29, 1987